Global soil organic carbon removal by water erosion under climate change and land use change during 1850-2005 AD

Victoria Naipal[1], Philippe Ciais[1], Yilong Wang[1], Ronny Lauerwald[2, 3], Bertrand Guenet[1], Kristof Van Oost[4]

[1]Laboratoire des Sciences du Climat et de l'Environnement, CEA CNRS UVSQ, Gif-sur-Yvette 91191, France
[2]Department of Geoscience, Environment & Society, Université Libre de Bruxelles, Brussels, Belgium
[3]Department of Mathematics, College of Engineering, Mathematics and Physical Sciences, University of Exeter, Exeter, UK
[4]Université catholique de Louvain,TECLIM - Georges Lemaître Centre for Earth and Climate Research, Louvain-la-Neuve, Belgium

Correspondence to: Victoria Naipal (victoria.naipal@lsce.ipsl.fr)

Abstract

The onset and expansion of agriculture has accelerated soil erosion by rainfall and runoff substantially, mobilizing vast quantities of soil organic carbon (SOC) globally. Studies show that at timescales of decennia to millennia this mobilized SOC can significantly alter previously estimated carbon emissions from land use change (LUC). However, a full understanding of the impact of erosion on land-atmosphere carbon exchange is still missing. The aim of our study is to better constrain the terrestrial carbon fluxes by developing methods compatible with Earth System Models (ESMs) in order to explicitly represent the links between soil erosion by rainfall and runoff and carbon dynamics. For this we use an emulator that represents the carbon cycle of a land surface model, in combination with the Revised Universal Soil Loss Equation model. We applied this modeling framework at the global scale to evaluate the effects of potential soil erosion (soil removal only) in the presence of other perturbations of the carbon cycle: elevated atmospheric CO_2, climate variability, and LUC. We found that over the period 1850-2005 AD acceleration of soil erosion leads to a total potential SOC removal flux of 100 Pg C of which 80% occurs on agricultural, pasture and natural grass lands. Including soil erosion in the SOC-dynamics scheme results in a doubling of the cumulative loss of SOC over 1850 – 2005 due to the combined effects of climate variability, increasing atmospheric CO_2 and LUC. This additional erosional loss decreases the cumulative global carbon sink on land by 5 Pg for this specific period, with the largest effects found for the tropics, where deforestation and agricultural expansion increased soil erosion rates significantly. We also show that the potential effects of soil erosion on the global SOC stocks cannot be ignored when compared to the effects of climate change or land use change on the carbon cycle. We conclude that it is necessary to include soil erosion in assessments of LUC and evaluations of the terrestrial carbon cycle.

1 Introduction

Carbon emissions from land use change (LUC), recently estimated as 1.0 ± 0.5 Pg C yr^{-1}, form the second largest
40   anthropogenic source of atmospheric CO_2 (Le Quéré *et al.*, 2016). However, their uncertainty range is large, making
it difficult to constrain the net land-atmosphere carbon fluxes and reduce the biases in the global carbon budget
(Goll *et al.,* 2017; Houghton and Nassikas, 2017; Le Quéré *et al.,* 2016). The absence of soil erosion in assessments
of LUC is an important part of this uncertainty, as soil erosion is strongly connected to LUC (Van Oost *et al.*, 2012;
Wang *et al.*, 2017).

45   The expansion of agriculture has accelerated soil erosion by rainfall and runoff significantly, mobilizing around 783
$\pm$ 243 Pg of soil organic carbon (SOC) globally over the past 8000 years (Wang *et al.*, 2017). Most of the mobilized
SOC is redeposited in alluvial and colluvial soils, where it is stabilized and buried for decades to millennia
(Hoffmann *et al.*, 2013a; Hoffmann *et al.*, 2013b; Wang *et al.*, 2017). Together with dynamic replacement of
removed SOC by new litter input at the eroding sites, and the progressive exposure of carbon-poor deep soils, this
50   translocated and buried SOC can lead to a net carbon sink at the catchment scale, potentially offsetting a large part
of the carbon emissions from LUC (Berhe *et al.*, 2007; Bouchoms *et al.*, 2017; Harden *et al.*, 1999; Hoffmann *et al.*,
2013a; Lal, 2003; Stallard, 1998; Wang *et al.*, 2017).

On eroding sites, soil erosion keeps the SOC stocks below a steady-state (Van Oost *et al.,* 2012) and can lead to
substantial CO_2 emissions in certain regions (Billings *et al.*, 2010; Worrall *et al.*, 2016; Lal, 2003). CO_2 emission
55   from soil erosion can take place during the breakdown of soil aggregates by erosion and during the transport of the
eroded SOC by runoff and later also by streams and rivers.

LUC emissions are usually quantified using bookkeeping models and land surface models (LSMs) that represent the
impacts of LUC activities on the terrestrial carbon cycle (Le Quere *et al.*, 2016) only through processes leading to a
local imbalance between NPP and heterotrophic respiration, ignoring lateral displacement. Currently, LSMs
60   consider only the carbon fluxes following LUC resulting from changes in vegetation, soil carbon and sometimes
wood products (Van Oost *et al.*, 2012; Stocker *et al.*, 2014). The additional carbon fluxes associated with the human
action of LUC from the removal and lateral transport of SOC by erosion are largely ignored.

In addition, the absence of lateral SOC transport by erosion in LSMs complicates the quantification of the human
perturbation of the carbon flux from land to inland waters (Regnier *et al.*, 2013). Recent studies have been
65   investigating the Dissolved Organic Carbon (DOC) transfers along the terrestrial-aquatic continuum in order to
better quantify CO_2 evasion from inland waters and to constrain the lateral carbon flux from the land to the ocean
(Lauerwald *et al.*, 2017; Regnier *et al.*, 2013). They point out that an explicit representation of soil erosion and
sediment transport – in addition to DOC leaching and transport - in future LSMs is essential to be able to better
constrain the flux from land to ocean. This is true, since the transfer of particulate organic carbon from eroded SOC
70   also matters for estimating carbon inputs to rivers.

The slow pace of carbon sequestration by soil erosion and deposition (Van Oost *et al.*, 2012; Wang *et al.*, 2017) and
the slowly decomposing SOC pools require the simulation of soil erosion at timescales longer than a few decades to

fully quantify its impacts on the SOC dynamics. This, and the high spatial resolution that soil erosion models typically require, complicates the introduction of soil erosion and related processes in LSMs.

75 Previous approaches used to explicitly couple soil erosion and SOC turnover have been applying different erosion and carbon dynamic models at different spatial and temporal scales. Some studies coupled process-oriented soil erosion models with C turnover models calibrated for specific micro-catchments on timescales of a few decades to a millennium, (Billings *et al.*, 2010; Van Oost *et al.*, 2012; Nadeu *et al.*, 2015; Wang *et al.*, 2015a; Zhao *et al.*, 2015; Bouchoms *et al.*, 2017). While other studies focused on the application of parsimonious erosion-SOC dynamics

80 models using the RUSLE approach together with sediment transport methods at regional or continental spatial scales (Chappell *et al*., 2015; Lugato *et al*., 2016; Yue *et al*., 2016; Zhang *et al*., 2014). However, the modeling approaches used in these studies apply erosion models that still require many variables and data input that is often not available at the global scale or for the past or the future time period. These models also run on a much higher spatial resolution than LSMs, making it difficult to integrate them with LSMs. The study of Ito (2007) was one of the first

85 studies to couple water erosion to the carbon cycle at the global scale, using a simple modelling approach that combined the RUSLE model with a global ecosystem carbon cycle model. However, there are several unaddressed uncertainties related to his modelling approach, such as the application of the RUSLE at the global scale without adjusting its parameters.

Despite all the differences between the studies that coupled soil erosion to the carbon cycle, they all agree that soil

90 erosion by rainfall and runoff is an essential component of the carbon cycle. Therefore, to better constrain the land-atmosphere and the land-ocean carbon fluxes, it is necessary to develop new LSM-compatible methods that explicitly represent the link between soil erosion and carbon dynamics at regional to global scales *and* over long timescales. Based on this, our study introduces a 4D modeling approach that consists of 1) an emulator that simulates the carbon dynamics like in the ORCHIDEE LSM (Krinner *et al*., 2005), 2) the Revised Universal Soil

95 Loss (Adj.RUSLE) model that has been adjusted to simulate global soil removal rates based on coarse resolution data input from climate models (Naipal *et al.*, 2015), and 3) a spatially explicit representation for LUC. This approach represents explicitly and consistently the links between the perturbation of the terrestrial carbon cycle by elevated atmospheric CO_2 and variability (temperature and precipitation change), the perturbation of the carbon cycle by LUC and the effect of soil erosion at the global scale.

100 The main goal of our study is to use this new modeling approach to determine the potential effects of long-term soil erosion by rainfall and runoff without deposition or transport on the global SOC stocks under LUC, climate variability and increasing atmospheric CO_2 levels. In order to be able to determine if global soil erosion is a net carbon source or sink, it is essential to study first how soil erosion, without deposition or transport, interacts with the terrestrial carbon cycle. Therefore, we also aim to understand the links between the different perturbations to the

105 carbon cycle in the presence of soil erosion and to identify relevant changes in the spatial variability of SOC stocks under erosion.

2 Materials and methods

110   **2.1 Modeling framework concept**

We used the LSM ORCHIDEE-MICT (Guimberteau *et al.*, 2017; Zhu *et al.*, 2016) (in the following simply referred to as ORCHIDEE) to construct a carbon emulator that describes the carbon pools and fluxes exactly as in ORCHIDEE. MICT stands for aMeliorated Interactions between Carbon and Temperature, and this version of
115   ORCHIDEE has several major modifications and improvements for especially the high-latitudes.

ORCHIDEE has 8 biomass pools, 4 litter pools, of which 2 are above-ground and 2 are below-ground and 3 SOC pools for each land cover type (Fig. 1A). It has been extensively validated using observations on energy, water and carbon fluxes at various eddy-covariance sites, and with measurements of atmospheric CO_2 concentration (Piao *et al*., 2009). The land cover types are represented by 12 plant functional types (PFT's) and an additional type for bare
120   soil. 10 PFT's represent natural vegetation and 2 represent agricultural land (C3 and C4 crop).

The turnover times for each of the PFT-specific litter and SOC pools depend on their residence time modified by local soil texture, humidity, and temperature conditions (Krinner *et al.*, 2005). Land use change is not taken into account in the simulations with the full ORCHIDEE model, but is represented offline by a LUC scheme in the emulator as described in the next section. This makes it possible to switch on or off the LUC module in the emulator
125   or to change LUC scenarios when needed without having to re-run the full ORCHIDEE model. The loss of biomass and litter carbon by fire is represented by the parameterization of the Spitfire model from Thonicke *et al.* (2011) in the full ORCHIDEE model, and currently cannot be modified in our version of the emulator. Carbon losses by fire here are considered to contribute directly to the CO_2 emissions from land.

This emulator, which imitates the behavior of the carbon cycle of ORCHIDEE, reduces the computation time of the
130   complex ORCHIDEE model significantly, because the computation of hydrological processes and other computationally expensive processes are not included in the emulator. At the same time the emulator preserves the structure of the carbon cycle of ORCHIDEE and is able to reproduce the outputs exactly as by the full ORCHIDEE model. Using the emulator allowed us to add and study erosion-related processes affecting the carbon dynamics of the soil without having to include an erosion module in the full ORCHIDEE model (Fig. 1A). At face value, the
135   emulator merely copies the ORCHIDEE carbon pool dynamics, and for each new atmospheric CO_2- and climate-scenario a new run of the original LSM is required.

The change in carbon over time for each pool of the original model is represented in the emulator by the following general mass-balance approach:

$$\frac{dC}{dt} = I(t) - k * C(t) \tag{1}$$

140   Here, $\frac{dC}{dt}$ represents the change in carbon stock of a certain pool over time, calculated by the difference between the incoming flux ($I(t)$), and the outgoing flux ($k*C(t)$) to the respective pool, where k is the turnover rate. Although originally calculated by complex equations, the dynamic evolution of each pool can be described using the first-order model of Eq. 1. For each carbon pool the carbon stock and all the incoming and outgoing fluxes are derived at a daily time step from a simulation performed with the full ORCHIDEE model. Based on the output stock and
145   fluxes, the values of the turnover rates are calculated and archived together with the input fluxes. They are then used

to perform simulations of the dynamics of all pools with the emulator without having to re-compute the carbon fluxes at each time-step.

ORCHIDEE also includes crop harvest, defined as the harvest of above-ground biomass of agricultural PFTs, and calculated based on the concept of the harvest index (Krinner *et al.*, 2005). The harvest index is defined as the yield

150 of crop expressed as a fraction of the total above-ground dry matter production (Hay, 1995). ORCHIDEE uses a fixed harvest index for crop of 0.45. However, Hay (1995) showed that the harvest index has increased significantly since 1900 for C3 crop such as wheat. In the emulator, and also in the full ORCHIDEE model, the carbon balance of agricultural lands is sensitive to crop harvest. Based on this we use the findings of Hay (1995) to change the harvest index of C3 crops to be temporally variable over the period 1850 – 2005 in the emulator, with values ranging

155 between 0.26 and 0.46. This means that more crop biomass is harvested against what becomes litter. We only changed the HI of C3 plants, because Hay (1995) mentioned that C4 plants, such as maize, had already a high HI at the start of the last century. It should be noted that the harvest index does not vary spatially in our emulator, and harvesting is then done constantly at each time step.

160 **2.2 Net land use change**

To account for the effects of LUC, a net-land use change routine is implemented in the emulator that includes past agricultural and grassland expansion over natural PFTs (Fig. 1B). Fractions of PFT's in each grid cell are updated every year given prescribed annual maps of agricultural and natural PFTs (Peng *et al.*, 2017). The carbon stocks of

165 the litter and SOC pools of all the shrinking PFT's are then summed and allocated proportionally to the expanding or new PFT's, maintaining the mass-balance (Houghton and Nassikas, 2017; Piao *et al.,* 2009). When natural vegetation is reduced by LUC, the heartwood and sapwood biomass pools are harvested and transformed to 3 wood products with turnover times of 1 year, 10 years and 100 years. The other biomass pools (leafs, roots, sapwood below-ground, fruits, heartwood belowground) are transformed to metabolic or structural litter and allocated to the

170 respective litter pools of the expanding PFTs (Piao *et al.*, 2009).

2.3 Soil carbon dynamics

The change in the carbon content of the PFT-specific SOC pools in the emulator without soil erosion can be

175 described with the following differential equations:

$$\frac{dSOC_a(t)}{dt} = lit_a(t) + k_{pa} * SOC_p(t) + k_{sa} * SOC_s(t) - \left(k_{ap} + k_{as} + k0_a\right) * SOC_a(t) \quad (2)$$

$$\frac{dSOC_s(t)}{dt} = lit_s(t) + k_{as} * SOC_a(t) - \left(k_{sa} + k_{sp} + k0_s\right) * SOC_a(t) \quad (3)$$

$$\frac{dSOC_p(t)}{dt} = k_{ap} * SOC_a(t) + k_{sp} * SOC_s(t) - \left(k_{pa} + k0_p\right) * SOC_p(t) \quad (4)$$

where SOC_a, SOC_s, and SOC_p (g C m^{-2}) are the active (unprotected), slow (physically or chemically protected) and

180 passive (biochemically recalcitrant) SOC, respectively. The active SOC pool has the lowest residence time and the passive the highest. lit_a and lit_s (g C m^{-2} day^{-1}) are the litter input rates to the active and slow SOC pools,

respectively; $k0_a$, $k0_s$ and $k0_p$ (day^{-1}) are the respiration rates of the active, slow and passive pools, respectively; k_{as}, k_{ap}, k_{pa}, k_{sa}, k_{sp} are the coefficients determining the flux from the active to the slow pool, from the active to the passive pool, from the passive to the active pool, from the slow to the active pool and from the slow to the passive

185 pool, respectively (Fig. 1A).

The SOC pools are not vertically discretized in this model version of ORCHIDEE, so we implemented a simple vertical discretization scheme for the SOC pools in the emulator based on the concept of Wang *et al.* (2015a,b). In this scheme the carbon dynamics of each soil layer are calculated separately, based on layer dependent input and respiration rates (Fig. 1A). We apply the same vertical discretization scheme for all three SOC pools, assuming that

190 the different SOC pools are distributed across all layers of the soil profile. Also, we do not include processes such as bioturbation or leaching of litter or SOC.

In the emulator, the soil profile is divided into layers of 1 cm thickness down to a depth of 2 m, which is the soil depth used by ORCHIDEE to calculate SOC. The first 10 cm of the soil profile are referred to as the "topsoil", where we assume that the SOC content is homogeneously distributed. The rest of the soil profile is referred to as the

195 subsoil. The topsoil receives carbon from above- and below-ground litter, and each of the soil layers in the topsoil receives an equal fraction of both litter types. The SOC respiration rates for the topsoil layers are equal to those from ORCHIDEE and are determined by average soil temperature, moisture and texture. For the rest of the soil profile the respiration rates of all three SOC pools decrease exponentially with depth:

$$k_i(z) = k_{0\,i} * e^{-r_e z} \tag{5}$$

200 Here $k_{0\,i}$ is the SOC respiration rate at the surface layer for each SOC pool (i = a, s, p) as derived by the emulator based on the original ORCHIDEE rates. r_e (m^{-1}) is an exponential decreasing coefficient representing the impact of external factors, such as oxygen availability, reducing SOC mineralization rate with depth (z). After performing sensitivity simulations where the values of r_e differ per PFT, we found no significant difference in the resulting SOC stocks. The value of r_e was then set to 1.2 m^{-1}, so that the respiration rate decreases with a factor of 2-3 from the

205 surface to 1 m depth consistent with SOC profile observations (Bouchoms *et al*., 2017; Van Oost *et al*., 2005; Wang *et al*., 2015a). This vertical discretization in the emulator leads to a total global SOC stock that is approximately 44% larger than that from the original ORCHIDEE model, because it affects the mean value of the decomposition rates.

The below-ground litter input for the active SOC pool is the sum of a fraction of the below-ground structural and

210 metabolic litter pools from ORCHIDEE, while the below-ground litter input for slow SOC pool is equal to a fraction of the below-ground structural litter pool only. This setting is consistent with the structure of the SOC module of ORCHIDEE. We assume that the subsoil receives carbon only from below-ground litter, and that this input decreases exponentially with depth following the root profile of ORCHIDEE. This discretization of the total below-ground litter input (lit_{be}) is the same for both SOC pools and can then be represented as:

215 $$lit_{be} = \int_{z=0}^{z=z_{max}} I_{0be} * e^{-r*z} \, dz \tag{6}$$

where I_{0be} is the below-ground litter input to the surface layer, and is equal to:

$$I_{0be} = lit_{be} * \frac{r}{1-e^{-r*z_{max}}} \tag{7}$$

The homogeneously distributed below-ground litter input (I_{be}) to the layers of the topsoil is equal to:

$$\frac{\sum_{z=0}^{z=10} I_{be0} * e^{-r*z}}{0.1} \qquad (8a)$$

220   The below-ground litter input to the layers of the subsoil is equal to:

$$I_{be}(z) = I_{be0} * e^{-r*z} \qquad (8b)$$

where z_{max} is the maximum soil depth equal to 2 m, and dz is the soil layer discretization (1 cm); r is the PFT-specific vertical root-density attenuation coefficient as used in ORCHIDEE (Table S2).

225   The annual average soil erosion rate (E, t ha^{-1} year^{-1}) is calculated by the Adj.RUSLE (Naipal et al., 2015; Naipal et al., 2016) according to:

$$E = S * R * K * C \qquad (9)$$

where R is the rainfall erosivity factor (MJ mm ha^{-1} h^{-1} year^{-1}), K is the soil erodibility factor (t ha h ha^{-1} MJ^{-1} mm^{-1}), C is the land cover factor (dimensionless), S is the slope steepness factor (dimensionless). The S-factor is calculated

230   using the slope from a 1km resolution digital elevation model (DEM) that has been scaled using the fractal method to a resolution of 150m (Naipal *et al.,* 2015). In this way the spatial variability of a high-resolution slope dataset can be captured. The computation of the R factor has been adjusted to use coarse resolution input data on precipitation and to provide reasonable global erosivity values. For this Naipal *et al.* (2015) derived regression equations for different climate zones of the Köppen–Geiger climate classification (Peel *et al.*, 2007). The results from the

235   Adj.RUSLE model have been tested against empirical large-scale assessments of soil erosion and rainfall erosivity (Naipal *et al.,* 2015, 2016). The original RUSLE model as described by Renard *et al.* (1997) also includes the slope-length (L) and support-practice (P) factors. Although these factors can strongly affect soil erosion in certain regions, the Adj.RUSLE does not include these factors due to several reasons. Firstly, (Doetterl *et al.*, 2012) showed that these factors do not significantly contribute to the variation in soil erosion at the continental to global scales, in

240   comparison to the other RUSLE factors. Secondly, data on the L and P factors and methods to estimate them at the global scale are very limited. Thus, including them in global soil erosion estimations would result in large uncertainties. Finally, the focus of this study is to show the effects of potential soil erosion on the terrestrial carbon cycle, without the explicit effect of management practices such as covered by the P-factor. For more information on the validation of our erosivity values and a more detailed description of the calculation of each of the RUSLE factors

245   see S1.

The Adj. RUSLE model is not imbedded in the C emulator but is run separately on a 5arcmin spatial resolution and at a yearly timestep. The resulting soil erosion rates are then read by the C emulator at each time step and used to calculate the daily SOC erosion rate of a certain SOC pool i (Ce_i in g C m^{-2} day^{-1}) at the surface layer by:

$$Ce_i = SOC_i * \frac{\frac{E}{365} * 100}{BD_{top} * dz * 10^6} \qquad (10)$$

250   where BD_{top} is the bulk density of the surface layer (g cm^{-3}). We assume that the enrichment ratio, i.e. the volume ratio of the carbon content in the eroded soil to that of the source soil material, is equal to 1 here, which implies that our estimates of SOC mobilization are likely conservative (Chappell *et al*., 2015; Nadeu *et al.*, 2015).

When erosion takes place, the surface layer is truncated by the erosion height, and at the same time an amount of SOC corresponding to this erosion height is removed. As we assume that the soil layer thickness does not change,

255   part of the SOC of the next soil layer is allocated to the surface layer proportional to the erosion height and the SOC concentration (per volume) of the next layer. In this way, the SOC from all the following soil layers move upward and become exposed to erosion in the surface layer at some point in time (Fig. 1A). To preserve mass balance, we assume that there is no SOC below the 2 m soil profile represented in the emulator and new substrate replacing the material of the last soil layer is SOC free, so that SOC in the bottom layer will decrease towards zero after erosion

260   has started.

2.4 Input datasets

2.4.1 for ORCHIDEE

265

We used 6-hourly climate data supplied by CRU-NCEP (version 5.3.2) global database (https://crudata.uea.ac.uk/cru/data/ncep/) available at 0.5 degree resolution to perform simulations with the full ORCHIDEE model for constructing the emulator. CRU-NCEP climate data was only available for the period 1901-2012. To be able to run ORCHIDEE for the period 1850-1900, we randomly projected the climate forcing after 1900

270   to the years before 1900.

The PFT fractions were derived from the historical annual PFT maps developed by Peng *et al.* (2017). These PFT maps were available at a resolution of 0.25 degrees (Fig. 2), and were re-gridded to the resolution of the ORCHIDEE emulator, which is 2.5 x 3.75 degrees, using the nearest neighbor approach.

275   #### 2.4.2 for the Adj.RUSLE

Due to the the resolution of the Adj.RUSLE, which is 5 arcmin (~0.0833 degree), all the RUSLE factors had to be regridded or calculated at this specific resolution before calculating the soil erosion rates.

The land cover fractions from the historical 0.25 degree PFT maps were used in combination with the LAI values

280   from ORCHIDEE at the resolution of 2.5° x 3.75° to derive the values for the C-factor of the RUSLE model. We first regridded the yearly average LAI to the resolution of the PFT maps before calculating the land cover factor of RUSLE (C-factor) at the resolution of 0.25 degree. The C values were then regridded using the nearest neighbor method to the resolution of the Adj.RUSLE model. We used the nearest neighbor approach here, because the C-factor is strongly dependent on the land cover class.

285   Daily precipitation data for the period 1850-2005 to calculate soil erosion rates is derived from the Inter-Sectoral Impact Model Intercomparison Project (ISIMIP), product ISIMIP2b (Frieler *et al.*, 2017). This data is based on model output of the Coupled Model Intercomparison Project Phase 5 (CMIP5 output of IPSL-CM5A-LR (Taylor *et al.*, 2012), which are bias corrected using observational datasets and the method of Hempel *et al.* (2013), and made available at a resolution of 0.5 degrees (Fig. 2). We chose this data as input to the Adj.RUSLE model, because the

290   dataset extended to 1850, in contrast to the CRU-NCEP data. Also, this dataset being bias-corrected, provides a better distribution of extreme events and frequencies of dry and wet days (Frieler *et al.*, 2017), which is important

for the calculation of rainfall erosivity (R factor). The ISIMIP precipitation data was regridded using the bilinear interpolation method to the resolution of the Adj.RUSLE model, before being used to calculate the R-factor. This was necessary because the erosivity equations from the Adj.RUSLE model are calibrated at this specific resolution

295 (Naipal *et al.*, 2015).

Data on soil bulk density and other soil parameters to calculate the soil erodibility factor (K), available at the resolution of 1 km, have been taken from the Global Soil Dataset for use in Earth System Models (GSDE) (Shangguan *et al*, 2014). The K factor has been calculated at the resolution of 1 km before being regridded to 5 arcmin using the bilinear interpolation method. We also used the SOC concentration in the soil from GSDE, which

300 was derived using the "aggregating first" approach, to compare to our SOC stocks from simulations with the emulator. Finally, the slope steepness factor (S), which was originally estimated at the resolution of 1 km, was also regridded to the resolution of 5 arcmin using the bilinear interpolation method.

Using the above-mentioned data, soil erosion rates were first calculated at the resolution of 5 arcmin, and afterwards aggregated to the coarse resolution of the emulator (2.5° x 3.75°) to calculate daily SOC erosion rates.

305

2.5 Model simulations

To be able to understand and estimate the different direct and indirect effects of soil erosion on the SOC dynamics, we propose a factorial simulation framework (Fig. 3). This framework allows isolating or combining the main

310 processes that link soil erosion to the SOC pool, namely the influence from climate variability, LUC, and atmospheric CO_2 increase. The different model simulations described in this section will be based on this framework.

We performed two different simulations with the full ORCHIDEE model to produce the required data input for the emulator for the period 1850-2005. For this we first performed a spinup with ORCHIDEE to get stead-state carbon

315 pools for the year 1850. We chose the period 1850-2005 based on the ISIMIP2b precipitation data availability and the fact that this period underwent a significant intensification in agriculture globally and a substantial rise in atmospheric CO_2 concentrations. In the first simulation of ORCHIDEE the global atmospheric CO_2 concentration was fixed to the year 1850 to calculate time-varying NPP not impacted by CO2 fertilization and subsequent carbon pools, while in the second simulation the atmospheric CO_2 concentration was made variable. In both simulations,

320 climate is variable from CRU-NCEP (Fig. 3).

Furthermore, we performed three simulations with the Adj.RUSLE model to pre-calculate the soil erosion rates that will be used as input to the ORCHIDEE emulator. In the first simulation we kept the climate and land cover variable through time (the "CC+LUC" simulation). In the second simulation we only varied the climate through time and kept land cover fractions fixed to 1850 (the "CC" simulation, Fig. 3). In the third simulation we only varied the land

325 cover through time and kept the climate constant to the average cyclic variability of the period 1850-1859 (the "LUC" simulation, Fig. 3).

From the two simulations of ORCHIDEE (with variable and constant CO_2) and the soil erosion simulations of the Adj.RUSLE, we constructed 4 versions of the emulator to perform 8 simulations. The different simulations and their

description are given in table 1 and figure 3. In the simulations without LUC (S2, S4, S6 and S8), the PFT fractions
330   and the harvest index are constant and equal to those in the year 1850. In the simulations with LUC (S1, S3, S5 and
S7) the harvest index increases and the PFT fraction change with time during 1850 - 2005. In each emulator-
simulation we first calculated the equilibrium carbon stocks analytically before calculating the change of the carbon
stocks in time depending on the perturbations during the transient period (1851-2005). In simulations with erosion,
the equilibrium state of the SOC pools has been calculated using the average erosion rates of the period 1850-1859,
335   assuming erosion to be constant before 1850 and a steady state condition where erosion fluxes are equal to new
input from litter.

3 Results

340   **3.1 Erosion versus no erosion**

After including soil erosion in the ORCHIDEE emulator we obtain a total global soil loss flux of 47.6 Pg y^{-1} for the
year 2005 of which 29% is attributed to agricultural land and 54% to grassland (natural grass and pasture). This
global soil loss flux (here 'loss' meaning horizontal removal by erosion) leads to a total SOC loss flux of 0.67 Pg C
345   y^{-1} of which 31% are attributed to agricultural land and 60% to grassland (CTR, Fig 4). Grassland and agricultural
land thus have much larger annual average soil and SOC erosion rates compared to forest (Table 2).
The total soil and SOC losses in the year 2005 are an increase of 14% and 26.5%, respectively, compared to 1850
(CTR, Fig. 4) with the largest increases found in the tropics (Fig. 5B, D). The largest increase in soil and SOC
erosion during 1850 – 2005 is found in South-America (Table 3) despite of the significant decreases in simulated
350   precipitation leading to less intense erosion rates in this region. One should keep in mind that due to uncertainties in
the simulated LUC and climate variability for certain regions and the assumptions made in our modeling framework,
these trends in soil and SOC erosion rates are linked to some uncertainty. However, it is difficult to assess this
uncertainty, mainly due to the lack of observations for the past in regions such as the tropics and the lack of model-
testing in these regions.
355   We found that the total soil erosion flux on agricultural land almost doubled by the year 2005 compared to 1850,
while the SOC erosion flux increased by 62% (Fig. 4) and led to a cumulative SOC removal of 27 Pg on agricultural
land since 1850 (CTR). On pasture land and grassland, the soil erosion flux increased by only 8.5%, while the SOC
erosion flux increased by 34% (Fig. 4) and led to a cumulative SOC mobilization of 52 Pg since 1850. It is evident
that on agricultural land SOC erosion increases less strongly during 1850 – 2005 compared to soil erosion, while on
360   grassland the opposite effect is true. This is because in our model, LUC (without erosion) leads to a significant
increase in SOC on grassland, which amplifies the increasing trend in SOC erosion for grassland. This simulated
increase for SOC stocks on grasslands after LUC takes place is not unrealistic, as it is observed from paired
chronosequences worldwide that grasslands have higher SOC densities than forests for instance (Li *et al.*, 2017).
In total 7183 Pg of soil and 100 Pg of SOC is mobilized across all PFTs by erosion during the period 1850 - 2005,
365   which is equal to approximately 80% of the total net flux of carbon lost as CO_2 to the atmosphere due to LUC (net

LUC flux) over the same period estimated by our study (S1-S2). In this study, we do not address the fate of this large amount of eroded SOC, be it partly sequestered (Wang *et al.*, 2017) or released to the atmosphere as CO_2.

To estimate the net effect of soil erosion on the global SOC stocks under all perturbations we compare the cumulative SOC stock change from simulation S3 (no erosion; see Table 1) with that of the CTR simulation. When
370   assuming that the SOC mobilized by soil erosion in the CTR simulation is all respired (this is certainly an extreme and unrealistic assumption, as case in reality a fraction of mobilized SOC will remain stored on land, but we take this assumption as an extreme scenario) we find that the overall global SOC stock decrease would almost double during the period 1850 – 2005 compared to a world without soil erosion (Fig. 6A). The largest impact of including erosion in the SOC modeling scheme is observed for Asia, where the decrease in the total SOC stock is 9 times
375   larger when the effects of soil erosion are taken into account (Table 4, Fig. 8A). Some regions, such as West-Europe show instead a smaller SOC loss when erosion is taken into account. This is because we assume a steady state in 1850, where carbon losses by erosion are equal to the carbon input by litter. And as soil erosion decreased during 1850 - 2005 for Western Europe, mainly due to a decreasing trend in precipitation since 1965 and less intense expansion of agricultural- and grasslands (Fig. 5B), it partly offsets the decrease of SOC by LUC (Fig. 8).

380

3.2 Validation of model results

We calculated a total global SOC stock for 2005 in the absence of soil erosion (S3) of 2589 Pg, which is a factor of 1.48 higher than the total SOC stock from GSCE (Shangguan *et al.*, 2014) for a soil depth of 2m (Table 5). SOC
385   stocks of forest in our model contribute the most to this overestimation. We find that SOC stocks of agricultural land show the best comparison to the stocks of the GSDE dataset (Table S3). Including soil erosion (S1) leads to a total SOC stock of 1936 Pg for the year 2005 (Table 5). We also find that including soil erosion in the SOC-dynamics scheme slightly improves the root mean square error (RMSE) between the simulated SOC stocks and those from GSDE, especially for the top 30cm of the soil profile. This improvement in the RMSE occurs especially in highly
390   erosive areas. However, there are still large differences between our simulated SOC stocks and those from GSDE due to large uncertainties in the simulation of underlying processes that govern the SOC dynamics (Todd-Brown *et al.*, 2014) and missing SOC transport and deposition after erosion. Furthermore, the total SOC stock of agricultural land is significantly lower than of the GSDE, because we assume a steady-state landscape at 1850, where soil erosion losses are equal to the carbon input to the soil.
395   Using the Adj.RUSLE model to estimate agricultural soil loss by water erosion for the year 2005 resulted in a global soil loss flux of 14 Pg y^{-1} (Fig. 4). This flux is paralleled by a SOC loss flux of 0.19 Pg C y^{-1} after including soil erosion in the CTR simulation (Fig. 4). This soil loss flux is in the same order of magnitude as earlier high-resolution assessments of this flux, while the SOC removal flux is slightly lower compared to previously published high-resolution estimates, but within the uncertainty (Table 6). We also find a fair agreement between our model
400   estimates of recent agricultural soil and SOC erosion fluxes per continent and the high-resolution estimates (excluding tillage erosion) from the study of Doetterl *et al.* (2012) (Table 7). However, the continental SOC erosion fluxes from our study are generally lower, because of the lower SOC stocks on agricultural land. Only South-

America shows a higher SOC flux for present-day compared to the high-resolution estimates of Doetterl *et al.* (2012), which is the result of the simulated high productivity of crops in the tropics.

405 Furthermore, we find a cumulative soil loss of 1888 Pg and cumulative SOC removal flux of 27 Pg from agricultural land over the entire time period (CTR simulation). This soil loss flux lies in the range of 2480±720 Pg found by Wang *et al.* (2017) for the same time period, while the SOC removal flux is significantly lower than the 63 ± 19 Pg C found by Wang *et al.* (2017) . Wang *et al.* (2017) used only recent climate data in his study while we explicitly include the effects of changes in precipitation and temperature on global soil erosion rates and the SOC stocks in our

410 study, which may explain this difference.

4 Discussions

4.1 Significance of including soil erosion in the ORCHIDEE emulator

415

The significantly smaller increase in SOC stocks on agricultural land and grassland when soil erosion is taken into account (Fig. 7) explains the much higher decrease in the global SOC stock during 1850 – 2005 compared to a world without soil erosion (Fig. 6A). Due to the slow response of the global SOC stocks to perturbations, this impact of soil erosion can be even larger at longer timescales. The effect of soil erosion on the SOC stocks is also influenced

420 by the mechanism where removal of SOC causes a sink in soils that tend to return to equilibrium.

Furthermore, we find that the variability in the temporal trend of global SOC erosion is mainly determined by the variability in soil erosion rates and less by climate and rising atmospheric CO_2 that are affecting SOC stocks (Fig. 4). Also the spatial variability in SOC erosion rates for the year 2005 and the spatial variability in the change of SOC erosion during 1850 – 2005 follow closely the spatial variability of soil erosion rates (Fig. 5B, D). This can be

425 explained by the slow response of the SOC pools to changes in NPP and decomposition caused by CO_2 and climate in contrast to the fast response of soil erosion to changes in land cover and climate.

4.2 LUC versus precipitation and temperature change

430 Although the variability in the temporal trends of soil and SOC erosion is dominated by the variability in precipitation changes, the overall trend follows the increase in agricultural land and grassland.

If we separate the effects of LUC and climate variability co-varying with soil erosion we find that in the "LUC" erosion scenario with constant climate (see section 2.5), the total global soil loss from erosion increases by a factor of 1.27 since 1850, while in the "CC" erosion scenario with constant LUC the soil loss flux from erosion decreases

435 by a factor of 1.12 (Fig 4). Analyzing the effects of LUC and climate variability separately on SOC erosion we find that in the LUC-only scenario (S2-S1) the total global SOC loss increases by a factor of 1.35 since 1850, while in the climate-change-only scenario (S2) SOC loss decreases by a factor of 1.12 (Fig 4). This shows that LUC slightly dominates the trend in both soil and SOC erosion fluxes on the global scale during 1850 - 2005.

For soil erosion, however, LUC dominates the temporal trend less than for SOC erosion. This effect is especially
440   clear for grasslands, where we find that climate variability offsets a large part of the increase in soil erosion rates by
LUC, but not in the case of SOC erosion. This is the due to the fact that LUC has a much stronger effect on the
carbon content in the soil than the effect of climate and CO_2 change on the timescale of the last 200 years. Also,
intense soil erosion is typically found in mountainous areas where climate variability has significant impacts, while
at the same time these regions are usually poor in SOC.

445   Regionally, there are significant differences in the relative contributions of LUC versus climate variability to the
total soil erosion flux (Fig. 2 & 5). In the tropics in South-America, Africa and Asia, where intense LUC
(deforestation and expansion of agricultural areas) took place during 1850 - 2005, a clear increase in soil erosion
rates is found even in areas with a significant decrease in precipitation due to a higher agricultural area being
exposed to erosion. However, in regions where agriculture is already established and has a long history, precipitation
450   changes seem to have more impact than LUC on soil erosion rates. A combination of our assumption that erosion
rates are in steady state with carbon input to the soil at 1850, and minimal agricultural expansion during the last 200
years may be the reasons for this observation.

We also find that summing up the changes in soil erosion rates due to LUC alone and the changes in soil erosion due
to climate variability alone do not exactly match the results in the changes in soil erosion obtained when LUC and
455   climate variability are combined (Fig. 4). The non-linear differences between soil erosion rates calculated with
changing land cover fractions in combination with a constant climate ("LUC"), and soil erosion rates calculated by
subtracting the erosion simulation "CC" from "CC+LUC" are significant for agricultural land but much smaller for
other PFTs and at the global scale. It implies that the LUC effect on erosion depends on the background climate.
This is important to keep in mind when evaluating the LUC effect on SOC stocks in the presence of soil erosion.

460   The decrease in global SOC stocks in simulation S3 are due to the various effects of LUC (without erosion) (Fig.
6A). During 1850 – 2005 LUC has led to a decrease in natural vegetation and an increase in agricultural land. At the
global scale, the replacement of natural PFTs by crop results in increased SOC decomposition and decreased carbon
input to the soil by litter-fall due to harvest and a lower productivity. Regionally this effect of LUC may be different,
depending for example on the natural PFTs that are replaced. Furthermore, the increase in carbon input into the soil
465   after LUC due to increased litter fall when natural vegetation is removed may play a role, but this effect is only
temporary. In addition, wood harvest after deforestation and crop harvest contribute to the decreased carbon input to
the soils.

We find that globally the SOC stocks decrease by 34 Pg due to LUC only during 1850 – 2005 (Fig. 6A, S3-S4). The
overall change in carbon over this period summed up over all biomass, litter, SOC, and wood-product pools due to
470   LUC without erosion is a loss of 118 Pg C, which lies in the range of cumulative carbon emissions by LUC from
estimates of previous studies (Houghton and Nassikas, 2017; Li et al., 2017; Piao et al., 2009). The increase in soil
erosion by expanding agricultural- and grasslands (S1-S2) amplifies the decrease of SOC stocks implied by LUC in
absence of erosion (S3-S4) by 7 Pg or a factor of 1.2 (Fig. 6A). This leads to a total change in the overall carbon
stock on land of -125 Pg. Regionally the amplification of the LUC effect on SOC stocks by the increase in soil
475   erosion ranges between factor of 0.9 and 1.6 (Table 4).

Regionally, changes in precipitation can amplify or offset a large part of the increase in soil erosion due to LUC (Fig. 2 & 5E). Globally we find that the decrease in global total precipitation, especially in the Amazon after 1960AD, partly offsets the increase in soil loss due to land use change (Fig. 4). It should be noted that the uncertainty in precipitation from global climate models for the Amazon is significant making this result uncertain

480   (Mehran *et al.*, 2014). Furthermore, we find that precipitation and temperature changes lead to a small net decrease in SOC stocks at the global scale since 1950 (Fig. 9, S8). This is likely related to the decreased productivity under drought stress (Piao *et al*., 2009). However, soil erosion offsets this decrease by a small net increase of 2 Pg in SOC stocks, mostly due to the decreasing trend in precipitation globally after 1950 AD.

485   **4.3 Effects of atmospheric CO_2 increase**

In the ORCHIDEE model, increasing CO_2 leads to a fertilization effect as it increases the NPP, and results in a significant increase in biomass production on land for most PFTs, depending on the temperature and moisture conditions (Arneth *et al.*, 2017; Piao *et al.*, 2009). Figure 9 shows the contribution of this fertilization effect to the

490   cumulative SOC stock change during 1850 – 2005 (S4-S8), which is in the same order of magnitude as the effect of LUC excluding soil erosion. Together with climate variability the atmospheric CO_2 increase offsets all the carbon losses by LUC in our model, and leads even to a net cumulative sink of carbon on land over this period of about 28 Pg C (S3). This value is calculated by summing up the changes in all the biomass, litter and SOC pools, and is in line with other assessments that found a net carbon balance that is close to neutral over 1850 - 2005 (Arora *et al*.,

495   2011; Ciais *et al*., 2013; Khatiwala *et al.*, 2009).

In the presence of soil erosion, climate variability and the atmospheric CO_2 increase lead to a slightly smaller net cumulative sink of carbon over land of 23 Pg C (S1), still within the uncertainty of assessed estimates (Arora *et al.*, 2011; Ciais *et al.*, 2013; Khatiwala *et al.*, 2009).

When the CO_2 fertilization effect is absent (S5, S7), we find that the temporal trend in the cumulative change of

500   global SOC stocks is largely determined by the effect of LUC (Fig. 6B), and leads to a cumulative source of carbon on land of 92 Pg C. LUC alone leads to a cumulative decrease in SOC stocks of -29 Pg (S7-S8), which is 5 Pg less than the decrease in SOC stocks due to LUC in the presence of increasing atmospheric CO_2 concentrations (S3-S4). The overall change in carbon over 1850-2005 summed up over all biomass, litter and SOC pools due to LUC alone is -99 Pg C in absence of increasing CO_2 (S7-S8), which is 19 Pg less than the LUC effect on carbon stocks under

505   variable atmospheric CO_2 (S3-S4). LUC has indeed a smaller effect on carbon stocks in the absence of increasing CO_2 concentrations as expected, because the productivity of the vegetation is lower (lower NPP) resulting in less biomass that can be removed by deforestation.

The previously calculated global total soil erosion flux of 47.6 Pg y^{-1} leads to an annual SOC erosion flux of 0.65 Pg C y^{-1} in the year 2005 in the absence of increasing atmospheric CO_2 (S5), which is 0.02 Pg C y^{-1} less than the SOC

510   erosion flux under increasing CO_2 (S1). The global cumulative SOC loss over the entire time period in the absence of increasing atmospheric CO_2 is 2 Pg C less (S5). Although these changes in SOC are small, the effect of LUC on the SOC stocks is amplified by erosion with a factor of 1.27 in absence of increasing CO_2 (S5-S6), which is

significantly larger than the effect of LUC with increasing CO_2 (S1-S2). This means that the LUC effect in combination with soil erosion has a stronger effect on SOC stocks losses under constant atmospheric CO_2

515 conditions, because the CO_2 fertilization effect does not replenish SOC in agricultural lands everywhere.

4.4 Model limitations and next steps

One of the uncertainties related to our modeling approach is the aggregation of the high-resolution soil erosion rates

520 from the Adj.RUSLE model to the resolution of the emulator, which is needed because of the coarse resolution of ORCHIDEE and the limited computational power. In this way, we might not capture correctly the hotspots of carbon erosion and their effects on the local SOC dynamics in these regions.

In addition, our soil erosion model is limited to water erosion only. This might result in biases for regions where other types of soil erosion are dominant such as, tillage erosion (Van Oost *et al.*, 2007), gully erosion and landslides

525 (Hilton *et al.*, 2008; Hilton *et al.*, 2011; Valentin *et al.*, 2005).

Although our erosion model runs on a daily time step, the soil erosion rates are calculated on a yearly time step, and thus we might miss extreme climate events triggering large soil losses. In addition, the Adj.RUSLE is not trained for extreme events. The effect of precipitation and temperature change on the SOC stocks under soil erosion might thus be larger than in our model simulations.

530 Concerning the reconstructed PFT maps, only expansion and abandonment of agriculture is taken into account, but not soil conservation measures as implemented in Australia and the US to prevent erosion (Chappell *et al.*, 2012; Houghton *et al.*, 1999). Regarding the land use change method that we applied, we only account for net land use change and do not account for shifting cultivation or distinguish between areas that have already seen LUC. Forest regrowth and forest age are also not considered, which could bring uncertainties in our estimates of LUC emissions

535 (Yue *et al.*, 2017).

Finally, the ORCHIDEE model lacks processes such as nitrogen and phosphorus limitations and priming, which affect the productivity and SOC decomposition (Goll *et al.*, 2017; Guenet *et al.*, 2016).

5 Conclusions

540

In this study we introduced a 4D modeling approach where we coupled soil erosion to the C-cycle of ORCHIDEE and analyzed the potential effects of soil erosion, without sediment deposition or transport, on the global SOC stocks over the period 1850 – 2005. To calculate global potential soil erosion rates we used the Adj.RUSLE model that includes scaling approaches to calculate soil erosion rates at a coarse spatial and temporal resolution. The SOC

545 dynamics are represented by an emulator that imitates the behavior of the carbon cycle of the ORCHIDEE LSM and enables us to easily couple our soil erosion model to the C-cycle and calculate the effects of soil erosion under different climatic and land use conditions. Although our modeling approach is rather coarse and fairly simple, we found a fair agreement of our soil loss and SOC loss fluxes for the year 2005 with high-resolution estimates from other studies.

550   When applying the model on the time period 1850-2005 we found a total soil loss flux of 7183, where soil erosion rates increased strongest on agricultural land. This potential soil loss flux mobilized 100 Pg of SOC across all PFTs, which compares to 80% of the total net flux of carbon lost as CO_2 to the atmosphere due to LUC estimated by our study for the same time period. When assuming that all this SOC mobilized is respired we find that the overall SOC change over the period 1850-2005 would double. The effect of soil erosion on the cumulative SOC change between

555   1850 - 2005 differs significantly between regions, where the largest decrease in SOC due to soil erosion is found in Asia. The expansion of agricultural and grassland is the main driver behind the decreasing SOC stocks by soil erosion. Including soil erosion in the SOC dynamics amplifies the decrease in SOC stocks due to LUC by a factor of 1.2. Overall, the potential effects of soil erosion on the global SOC stocks show that soil erosion needs to be included in future assessments of the terrestrial C-cycle and especially LUC.

560

Data availability: Upon request from the authors

Author contribution

565   VN, PC, BG, designed the research, VN, PC, RL and YW performed the research, VN and YW performed the model simulations and data analysis, and all authors wrote the paper. The authors have no conflict of interest to declare.

Acknowledgements

570

Funding was provided by the Laboratory for Sciences of Climate and Environment (LSCE), CEA, CNRS and UVSQ. RL acknowledges funding from the European Union's Horizon 2020 research and innovation program under grant agreement no.703813 for the Marie Sklodowska-Curie European Individual Fellowship "C-Leak". PC acknowledges support from the European Research Council Synergy grant ERC-2013-SyG-610028 IMBALANCE-

575   P. We also thank A.Chappell and D.S.Goll for their useful comments during the early stages of this research, and D.Zhu for helping out with the model simulations.

References

580   Arneth, A., Sitch, S., Pongratz, J., Stocker, B. D., Ciais, P., Poulter, B., Bayer, A. D., Bondeau, A., Calle, L., Chini, L. P., Gasser, T., Fader, M., Friedlingstein, P., Kato, E., Li, W., Lindeskog, M., Nabel, J. E. M. S., Pugh, T. A. M., Robertson, E., Viovy, N., Yue, C. and Zaehle, S.: Historical carbon dioxide emissions caused by land-use changes are possibly larger than assumed, Nat. Geosci., 10(January), doi:10.1038/NGEO2882, 2017.

Arora, V. K., Scinocca, J. F., Boer, G. J., Christian, J. R., Denman, K. L., Flato, G. M., Kharin, V. V, Lee, W. G.

585   and Merryfield, W. J.: Carbon emission limits required to satisfy future representative concentration pathways of greenhouse gases, Geophys. Res. Lett., 38, L05805, doi:10.1029/2010GL046270, 2011.

Berhe, A. A., Harte, J., Harden, J. W. and Torn, M. S.: The Significance of the Erosion-induced Terrestrial Carbon Sink, Bioscience, 57(4), 337–346, 2007.

Billings, S. A., Buddemeier, R. W., DeB. Richter, D., Van Oost, K. and Bohling, G.: A simple method for

590   estimating the influence of eroding soil profiles on atmospheric CO2, Global Biogeochem. Cycles, 24(2), 1–14, doi:10.1029/2009GB003560, 2010.

Bouchoms, S., Wang, Z., Vanacker, V., Doetterl, S. and Van Oost, K.: Modelling long-term soil organic carbon dynamics under the impact of land cover change and soil redistribution, CATENA, doi:10.1016/j.catena.2016.12.008, 2017.

595   Chappell, A., Sanderman, J., Thomas, M. and Read, A.: The dynamics of soil redistribution and the implications for soil organic carbon accounting in agricultural south-eastern Australia, Glob. Chang. Biol., 18, 2081–2088, doi:10.1111/j.1365-2486.2012.02682.x, 2012.

Chappell, A., Baldock, J. and Sanderman, J.: The global significance of omitting soil erosion from soil organic carbon cycling schemes, Nat. Clim. Chang., (October), 1–5, doi:10.1038/NCLIMATE2829, 2015.

600   Ciais, P., Sabine, C., Bala, G., Bopp, L., Brovkin, V., Canadell, J., Chhabra, A., DeFries, R., Galloway, J., Heimann, M., Jones, C., Quéré, C. Le, Myneni, R. B., Piao, S. and Thornton, P.: Carbon and Other Biogeochemical Cycles, in Climate Change 2013: The physical science basis. Contribution of working group I to the fifth assessment report of the intergovernmental panel on climate change [Stocker, T.F., D. Qin, G.-K. Plattner, M. Tignor, S.K. Allen, J. Boschung, A. Nauels, Y. Xia, pp. 465–570, Cambridge University Press, Cambridge, United Kingdom and New

605   York, NY., 2013.

Doetterl, S., Van Oost, K. and Six, J.: Towards constraining the magnitude of global agricultural sediment and soil organic carbon fluxes, Earth Surf. Process. Landforms, doi:10.1002/esp.3198, 2012a.

Doetterl, S., Van Oost, K. and Six, J.: Towards constraining the magnitude of global agricultural sediment and soil organic carbon fluxes, Earth Surf. Process. Landforms, 37(6), 642–655, doi:10.1002/esp.3198, 2012b.

610   Frieler, K., Betts, R., Burke, E., Ciais, P., Denvil, S., Ebi, K., Eddy, T., Emanuel, K., Elliott, J., Galbraith, E., Simon, N., Halladay, K., Hattermann, F., Hickler, T., Hinkel, J., Mengel, M., Mouratiadou, I., Schmied, H. M., Vautard, R., Vliet, M. Van, Warszawski, L. and Zhao, F.: Assessing the impacts of 1 . 5 ° C global warming – simulation protocol of the Inter-Sectoral Impact Model Intercomparison Project (ISIMIP2b), Geosci. Model Dev. Discuss., (October), 1–59, doi:10.5194/gmd-2016-229, 2016.

615   Frieler, K., Lange, S., Piontek, F., Reyer, C. P. O., Schewe, J., Warszawski, L., Zhao, F., Chini, L., Denvil, S., Emanuel, K., Geiger, T., Halladay, K., Hurtt, G., Mengel, M., Murakami, D., Ostberg, S., Popp, A. and Riva, R.: Assessing the impacts of 1 . 5 ◦ C global warming – simulation protocol of the Inter-Sectoral Impact Model Intercomparison Project (ISIMIP2b), Geosci. Model Dev., 10, 4321–4345, 2017.

Goll, D. S., Winkler, A. J., Raddatz, T., Dong, N., Colin Prentice, I., Ciais, P. and Brovkin, V.: Carbon-nitrogen

620   interactions in idealized simulations with JSBACH (version 3.10), Geosci. Model Dev., 10(5), 2009–2030, doi:10.5194/gmd-10-2009-2017, 2017.

Guenet, B., Moyano, F. E., Peylin, P., Ciais, P. and Janssens, I. A.: Towards a representation of priming on soil carbon decomposition in the global land biosphere model ORCHIDEE (version 1 . 9 . 5 . 2), Geosci. Model Dev.,

9, 841–855, doi:10.5194/gmd-9-841-2016, 2016.

625   Guimberteau, M., Zhu, D., Maignan, F., Huang, Y., Yue, C., Dantec-N?d?lec, S., Ottl?, C., Jornet-Puig, A., Bastos,
A., Laurent, P., Goll, D., Bowring, S., Chang, J., Guenet, B., Tifafi, M., Peng, S., Krinner, G., Ducharne, A., Wang,
F., Wang, T., Wang, X., Wang, Y., Yin, Z., Lauerwald, R., Joetzjer, E., Qiu, C., Kim, H. and Ciais, P.: ORCHIDEE-
MICT (revision 4126), a land surface model for the high-latitudes: model description and validation, Geosci. Model
Dev. Discuss., (revision 4126), 1–65, doi:10.5194/gmd-2017-122, 2017.

630   Harden, J. W., Sharpe, J. M., Parton, W. J., Ojima, D. S., Fries, T. L., Huntington, T. G. and Dabney, S. M.:
Dynamic replacement and loss of soil carbon on eroding cropland, Global Biogeochem. Cycles, 13(4), 885–901,
doi:10.1029/1999GB900061, 1999.

Hay R.K.M.: Harvest index: a review of its use in plant breeding and crop physiology, Ann. appl. Biol., 126, 197–
216, 1995.

635   Hempel, S., Frieler, K., Warszawski, L., Schewe, J. and Piontek, F.: A trend-preserving bias correction – the ISI-
MIP approach, Earth Syst. Dyn., 4, 219–236, doi:10.5194/esd-4-219-2013, 2013.

Hilton, R. G., Galy, A., Hovius, N., Chen, M., Horng, M. and Chen, H.: Tropical-cyclone-driven erosion of the
terrestrial biosphere from mountains, Nat. Geosci. Lett., 1, 759, doi:10.1038/ngeo333, 2008.

Hilton, R. G., Meunier, P., Hovius, N., Bellingham, P. J. and Galy, A.: Landslide impact on organic carbon cycling

640   in a temperate montane forest, Earth Surf. Process. Landforms, 1679(July), 1670–1679, doi:10.1002/esp.2191, 2011.

Hoffmann, T., Schlummer, M., Notebaert, B., Verstraeten, G. and Korup, O.: Carbon burial in soil sediments from
Holocene agricultural erosion, Central Europe, Global Biogeochem. Cycles, 27(3), 828–835,
doi:10.1002/gbc.20071, 2013a.

Hoffmann, T., Mudd, S. M., van Oost, K., Verstraeten, G., Erkens, G., Lang, a., Middelkoop, H., Boyle, J., Kaplan,

645   J. O., Willenbring, J. and Aalto, R.: Short Communication: Humans and the missing C-sink: erosion and burial of
soil carbon through time, Earth Surf. Dyn., 1(1), 45–52, doi:10.5194/esurf-1-45-2013, 2013b.

Houghton, R. A. and Nassikas, A. A.: Global and regional fluxes of carbon from land use and land cover change
1850–2015, Global Biogeochem. Cycles, 31(3), 456–472, doi:10.1002/2016GB005546, 2017.

Houghton, R. A., Hackler, J. L. and Lawrence, K. T.: The U . S . Carbon Budget : Contributions from Land-Use

650   Change, Science (80-.)., 285(July), 574–579, 1999.

Ito, A.: Simulated impacts of climate and land-cover change on soil erosion and implication for the carbon cycle,
1901 to 2100, Geophys. Res. Lett., 34(9), n/a-n/a, doi:10.1029/2007GL029342, 2007.

Khatiwala, S., Primeau, F. and Hall, T.: Reconstruction of the history of anthropogenic CO 2 concentrations in the
ocean, Nature, 462(7271), 346–349, doi:10.1038/nature08526, 2009.

655   Krinner, G., Viovy, N., de Noblet-Ducoudré, N., Ogée, J., Polcher, J., Friedlingstein, P., Ciais, P., Sitch, S. and
Prentice, I. C.: A dynamic global vegetation model for studies of the coupled atmosphere-biosphere system, Global
Biogeochem. Cycles, 19(1), 1–33, doi:10.1029/2003GB002199, 2005.

Lal, R.: Soil erosion and the global carbon budget., Environ. Int., 29(4), 437–50, doi:10.1016/S0160-
4120(02)00192-7, 2003.

660   Lauerwald, R., Regnier, P., Camino-Serrano, M., Guenet, B., Guimberteau, M., Ducharne, A., Polcher, J. and Ciais,

P.: ORCHILEAK: A new model branch to simulate carbon transfers along the terrestrial-aquatic continuum of the Amazon basin, Geosci. Model Dev. Discuss., (April), doi:10.5194/gmd-2017-79, 2017.

Li, W., Ciais, P., Peng, S., Yue, C., Wang, Y., Thurner, M., Sassan, S., Arneth, A., Avitabile, V., Carvalhais, N., Harper, A. B., Kato, E., Koven, C., Liu, Y. Y., Nabel, J. E. M. S., Pan, Y., Pongratz, J., Poulter, B., Pugh, T. A. M.,
665   Santoro, M., Sitch, S., Stocker, B. D. and Viovy, N.: Land-use and land-cover change carbon emissions between 1901 and 2012 constrained by biomass observations, Biogeosciences Discuss., (June), doi:10.5194/bg-2017-186, 2017.

Lugato, E., Paustian, K., Panagos, P., Jones, A. and Borrelli, P.: Quantifying the erosion effect on current carbon budget of European agricultural soils at high spatial resolution, Glob. Chang. Biol., doi:10.1111/gcb.13198, 2016.
670   Mehran A., AghaKouchak A., and P. T. J.: Evaluation of CMIP5 continental precipitation simulations relative to satellite-based gauge-adjusted observations, J. Geophys. Res. Atmos., (119), 1695–1707, doi:10.1002/2013JD021152.Received, 2014.

Nadeu, E., Gobin, A., Fiener, P., van Wesemael, B. and van Oost, K.: Modelling the impact of agricultural management on soil carbon stocks at the regional scale: the role of lateral fluxes., Glob. Chang. Biol., 21(8), 3181–
675   92, doi:10.1111/gcb.12889, 2015.

Naipal, V., Reick, C., Pongratz, J. and Van Oost, K.: Improving the global applicability of the RUSLE model - Adjustment of the topographical and rainfall erosivity factors, Geosci. Model Dev., 8(9), doi:10.5194/gmd-8-2893-2015, 2015.

Naipal, V., Reick, C., Van Oost, K., Hoffmann, T. and Pongratz, J.: Modeling long-term, large-scale sediment
680   storage using a simple sediment budget approach, Earth Surf. Dyn., 4(2), doi:10.5194/esurf-4-407-2016, 2016.

Van Oost, K., Govers, G., Quine, T. a., Heckrath, G., Olesen, J. E., De Gryze, S. and Merckx, R.: Landscape-scale modeling of carbon cycling under the impact of soil redistribution: The role of tillage erosion, Global Biogeochem. Cycles, 19, GB4014, doi:10.1029/2005GB002471, 2005.

Van Oost, K., Quine, T. a, Govers, G., De Gryze, S., Six, J., Harden, J. W., Ritchie, J. C., McCarty, G. W.,
685   Heckrath, G., Kosmas, C., Giraldez, J. V, da Silva, J. R. M. and Merckx, R.: The impact of agricultural soil erosion on the global carbon cycle., Science, 318(5850), 626–9, doi:10.1126/science.1145724, 2007.

Van Oost, K., Verstraeten, G., Doetterl, S., Notebaert, B., Wiaux, F. and Broothaerts, N.: Legacy of human-induced C erosion and burial on soil – atmosphere C exchange, PNAS, 109(47), 19492–19497, doi:10.1073/pnas.1211162109/-/DCSupplemental.www.pnas.org/cgi/doi/10.1073/pnas.1211162109, 2012.
690   Peel, M. C., Finlayson, B. L. and Mcmahon, T. A.: Updated world map of the Koeppen-Geiger climate classification, Hydrol. Earth Syst. Sci., 11, 1633–1644, 2007.

Peng, S., Ciais, P., Maignan, F., Li, W., Chang, J., Wang, T. and Yue, C.: Sensitivity of land use change emission estimates to historical land use and land cover mapping, Global Biogeochem. Cycles, 31(4), 626–643, doi:10.1002/2015GB005360, 2017.
695   Piao, S., Ciais, P., Friedlingstein, P., De Noblet-Ducoudré, N., Cadule, P., Viovy, N. and Wang, T.: Spatiotemporal patterns of terrestrial carbon cycle during the 20th century, Global Biogeochem. Cycles, 23(4), 1–16, doi:10.1029/2008GB003339, 2009.

Le Quéré, C., Andrew, R. M., Canadell, J. G., Sitch, S., Ivar Korsbakken, J., Peters, G. P., Manning, A. C., Boden, T. A., Tans, P. P., Houghton, R. A., Keeling, R. F., Alin, S., Andrews, O. D., Anthoni, P., Barbero, L., Bopp, L.,

700   Chevallier, F., Chini, L. P., Ciais, P., Currie, K., Delire, C., Doney, S. C., Friedlingstein, P., Gkritzalis, T., Harris, I., Hauck, J., Haverd, V., Hoppema, M., Klein Goldewijk, K., Jain, A. K., Kato, E., Körtzinger, A., Landschützer, P., Lefèvre, N., Lenton, A., Lienert, S., Lombardozzi, D., Melton, J. R., Metzl, N., Millero, F., Monteiro, P. M. S., Munro, D. R., Nabel, J. E. M. S., Nakaoka, S. I., O'Brien, K., Olsen, A., Omar, A. M., Ono, T., Pierrot, D., Poulter, B., Rödenbeck, C., Salisbury, J., Schuster, U., Schwinger, J., Séférian, R., Skjelvan, I., Stocker, B. D., Sutton, A. J.,

705   Takahashi, T., Tian, H., Tilbrook, B., Van Der Laan-Luijkx, I. T., Van Der Werf, G. R., Viovy, N., Walker, A. P., Wiltshire, A. J. and Zaehle, S.: Global Carbon Budget 2016, Earth Syst. Sci. Data, 8(2), 605–649, doi:10.5194/essd-8-605-2016, 2016.

Quinton, J. N., Govers, G., Van Oost, K. and Bardgett, R. D.: The impact of agricultural soil erosion on biogeochemical cycling, Nat. Geosci., 3(5), 311–314, doi:10.1038/ngeo838, 2010.

710   Regnier, P., Friedlingstein, P., Ciais, P., Mackenzie, F. T., Gruber, N., Janssens, I. a., Laruelle, G. G., Lauerwald, R., Luyssaert, S., Andersson, A. J., Arndt, S., Arnosti, C., Borges, A. V., Dale, A. W., Gallego-Sala, A., Goddéris, Y., Goossens, N., Hartmann, J., Heinze, C., Ilyina, T., Joos, F., LaRowe, D. E., Leifeld, J., Meysman, F. J. R., Munhoven, G., Raymond, P. a., Spahni, R., Suntharalingam, P. and Thullner, M.: Anthropogenic perturbation of the carbon fluxes from land to ocean, Nat. Geosci., 6(8), 597–607, doi:10.1038/ngeo1830, 2013.

715   Shangguan H.W., Dai Y., Duan Q., Liu B., Y. H.: A global soil data set for earth systemmodeling Wei, J. Adv. Model. Earth Syst., 6, 249–263, doi:10.1002/2013MS000293.Received, 2014.

Stallard, R. F.: Terrestrial sedimentation and the carbon cycle : Coupling weathering and erosion to carbon burial, Global Biogeochem. Cycles, 12(2), 231–257, 1998.

Stocker, B. D., Feissli, F., Strassmann, K. M. and Spahni, R.: Past and future carbon fluxes from land use change,

720   shifting cultivation and wood harvest, Tellus B Chem. Phys. Meteorol., 66, 23188, doi:10.3402/tellusb.v66.23188, 2014.

Taylor, K. E., Stouffer, R. J. and Meehl, G. A.: A Summary of the CMIP5 Experiment Design, Am. Meteorol. Soc., 93, 485–498, doi:https://doi.org/10.1175/BAMS-D-11-00094.1, 2012.

Thonicke, K., Spessa, A., Prentice, I. C., Harrison, S. P. and Dong, L.: The influence of vegetation , fire spread and

725   fire behaviour on biomass burning and trace gas emissions : results from a process-based model, Biogeosciences, 7, 1991–2011, doi:10.5194/bg-7-1991-2010, 2010.

Todd-Brown, K. E. O., Randerson, J. T., Hopkins, F., Arora, V., Hajima, T., Jones, C., Shevliakova, E., Tjiputra, J., Volodin, E., Wu, T., Zhang, Q. and Allison, S. D.: Changes in soil organic carbon storage predicted by Earth system models during the 21st century, Biogeosciences, 11(8), 2341–2356, doi:10.5194/bg-11-2341-2014, 2014.

730   Valentin, C., Poesen, J. and Li, Y.: Gully erosion : Impacts , factors and control, CATENA, 63, 132–153, doi:10.1016/j.catena.2005.06.001, 2005.

Wang, Z., Doetterl, S., Vanclooster, M., van Wesemael, B. and Van Oost, K.: Constraining a coupled erosion and soil organic carbon model using hillslope-scale patterns of carbon stocks and pool composition, J. Geophys. Res. Biogeosciences, 120, doi:10.1002/2014JG002768, 2015a.

735   Wang, Z., Van Oost, K. and Govers, G.: Predicting the long-term fate of buried organic carbon in colluvial soils, Global Biogeochem. Cycles, doi:10.1002/2014GB004912, 2015b.

Wang, Z., Hoffmann, T., Six, J., Kaplan, J. O., Govers, G., Doetterl, S. and Van Oost, K.: Human-induced erosion has offset one-third of carbon emissions from land cover change, Nat. Clim. Chang., 7(5), 345–349, doi:10.1038/nclimate3263, 2017.

740   Worrall F., Burt T.P., H. N. J. K.: The fluvial flux of particulate organic matter from the UK: the emission factor of soil erosion, Earth Surf. Process. Landforms, 41(1), 61–71, 2016.

Yue, C., Ciais, P., Luyssaert, S., Li, W., Mcgrath, M. J., Chang, J. F., Peng, S. S. and Amsterdam, V. U.: Representing anthropogenic gross land use change , wood harvest and forest age dynamics in a global vegetation model ORCHIDEE-MICT (r4259), Geosci. Model Dev. Discuss. Model Dev. Discuss., 2017.

745   Yue, Y., Ni, J., Ciais, P., Piao, S., Wang, T., Huang, M., Borthwick, A. G. L., Li, T., Wang, Y., Chappell, A. and Van Oost, K.: Lateral transport of soil carbon and land-atmosphere CO_2 flux induced by water erosion in China, PNAS, 113(24), 6617–6622, doi:10.1073/pnas.1523358113, 2016.

Zhang, H., Liu, S., Yuan, W., Dong, W., Ye, A., Xie, X., Chen, Y., Liu, D., Cai, W. and Mao, Y.: Inclusion of soil carbon lateral movement alters terrestrial carbon budget in China, Sci. Rep., 4(7247), doi:10.1038/srep07247, 2014.

750   Zhao, J., Van Oost, K., Chen, L. and Govers, G.: Moderate topsoil erosion rates constrain the magnitude of the erosion-induced carbon sink and agricultural productivity losses on the Chinese Loess Plateau, Biogeosciences Discuss., 12(17), 14981–15010, doi:10.5194/bgd-12-14981-2015, 2015.

Zhu, D., Peng, S., Ciais, P., Zech, R., Krinner, G., Zimov, S. and Grosse, G.: Simulating soil organic carbon in yedoma deposits during the Last Glacial Maximum in a land surface model, Geophys. Res. Lett., 43(10), 5133–

755   5142, doi:10.1002/2016GL068874, 2016.

Table 1: Description of simulations used in this study. The S1 simulation is also the control simulation (CTR)

Simulation	Climate change	CO$_2$ change	Land use change	Erosion
S1	Yes	Yes	Yes	Yes
S2	Yes	Yes	No	Yes
S1-S2	No	Yes	Yes	Yes
S3	Yes	Yes	Yes	No
S4	Yes	Yes	No	No
S3-S4	No	Yes	Yes	No
S5	Yes	No	Yes	Yes
S6	Yes	No	No	Yes
S5-S6	No	No	Yes	Yes
S7	Yes	No	Yes	No
S8	Yes	No	No	No
S7-S8	No	No	Yes	No

Table 2: Area weighted average and standard deviation of soil and SOC erosion rates per PFT for the year 2005AD;
the low standard deviation for SOC erosion is due to the coarse resolution of the emulator

PFT	Mean soil erosion (t ha^{-1} y^{-1})	Standard deviation soil erosion (t ha^{-1} y^{-1})	Mean SOC erosion (kg C ha^{-1} y^{-1})	Standard deviation SOC erosion (kg C ha^{-1} y^{-1})
Crop	1.71	24.95	14	0.99
Grass	1.88	32.67	29	3.7
Forest	0.26	2.31	6.7	0.7

760   Table 3: Model estimates per continent of area-weighted average annual soil erosion and SOC erosion rates for the
year 2005, their spatial standard deviations, and the changes in average soil and SOC erosion rates since 1851; the
low standard deviation for SOC erosion is due to the coarse resolution of the emulator.

Region	Mean soil erosion rate	Standard deviation soil erosion rate	Change in mean soil erosion rate	Mean SOC erosion rate	Standard deviation SOC erosion rate	Change in mean SOC erosion rate
	2005	2005	2005 -1851	2005	2005	2005-1851
	(t ha^{-1} y^{-1})	(t ha^{-1} y^{-1})	(t ha^{-1} y^{-1})	(kg C ha^{-1} y^{-1})	(kg C ha^{-1} y^{-1})	(kg C ha^{-1} y^{-1})

Africa	2.69	68.47	0.69	21	2	7.3
Asia	6.03	167.83	0.23	75	12	5
Europe	2.45	73.70	0.48	21	5	2.1
Australia	1.46	16.98	-0.50	5	0.2	-0.6
South-America	4.69	117.58	1.35	86	18	38.4
North-America	2.83	63.68	0.15	45	9	4.4
Global	3.92	104.48	0.50	50	9.5	10.6

Table 4: Model estimates per continent of changes in SOC stocks since 1851 from simulations S1, S2, S1-S2, S3, S4, S3-S4

Region	Change SOC stocks S1	Change SOC stocks S2	Change SOC stocks S1-S2	Change SOC stocks S3	Change SOC stocks S4	Change SOC stocks S3-S4
	Pg C	Pg C	Pg C	Pg C	Pg C	Pg C
Africa	0.91	3.11	-2.2	1.35	2.79	-1.44
Asia	-2.53	12.74	-15.27	-0.29	11.08	-11.37
Europe	-2.68	2.98	-5.66	-3.38	3.08	-6.46
Australia	0.09	0.66	-0.57	0.24	0.66	-0.42
South-America	-0.91	5.9	-6.81	0.48	4.86	-4.38
North-America	-4.84	5.11	-9.95	-4.18	5.1	-9.28
Global	-9.96	30.5	-40.46	-5.78	27.57	-33.35

765   Table 5: Statistics of a grid cell by grid cell comparison of global SOC stocks between GSDE soil database and simulations S1 (with erosion) and S3 (without erosion). RMSE is the root mean square error and r-value is the correlation coefficient of the linear regression between GSDE and S1 of S3.

Soil depth (m)	GSDE SOC total (Pg)	S1 SOC total (Pg)	S3 SOC total (Pg)	RMSE S1	RMSE S3	r –value S1	r – value S3
0.3	670	742	1058	78.07	101.62	0.53	0.57
1	1356	1247	1677	126.39	155.63	0.59	0.58
2	1748	1936	2589	211.76	267.45	0.58	0.57

Table 6: Comparison of our model estimates of agricultural soil and SOC loss fluxes for the year 2005 with high-resolution model/observation estimates. *Quinton et al. (2010) included also pasture land in their study.

Study	Soil loss Pg y^{-1}	SOC loss Pg C y^{-1}
Van Oost et al. (2007)	17	0.25
Doetterl et al. (2012)	13	0.24
*Quinton et al. (2010)	28	0.5±0.15
Chappell et al. (2015)	17- 65	0.37 – 1.27
Wang et al. (2017)	17.7±1.70	0.44±0.06
This study	14	0.19

770   Table 7: Comparison of our model estimates of agricultural soil erosion and SOC erosion rates for the year 2005

with model/observation estimates from Doetterl et al. (2012) per continent

Region	*Our Study*		*Doetterl et al. (2012)*	
	Sediment flux 2005 Pg y^{-1}	SOC flux 2005 Tg C y^{-1}	Sediment flux 2000 Pg y^{-1}	SOC flux 2000 Tg C y^{-1}
Africa	2.6	29.0	2.4	39.5
Asia	5.4	71.0	4.9	90.0
Europe	2.1	36.5	1.9	39.5
Australia	0.2	1.3	0.3	4.3
South-America	1.6	37.5	1.4	26.7
North-America	0.7	17.0	1.6	31.5
Total	12.6	192.2	12.5	231.5
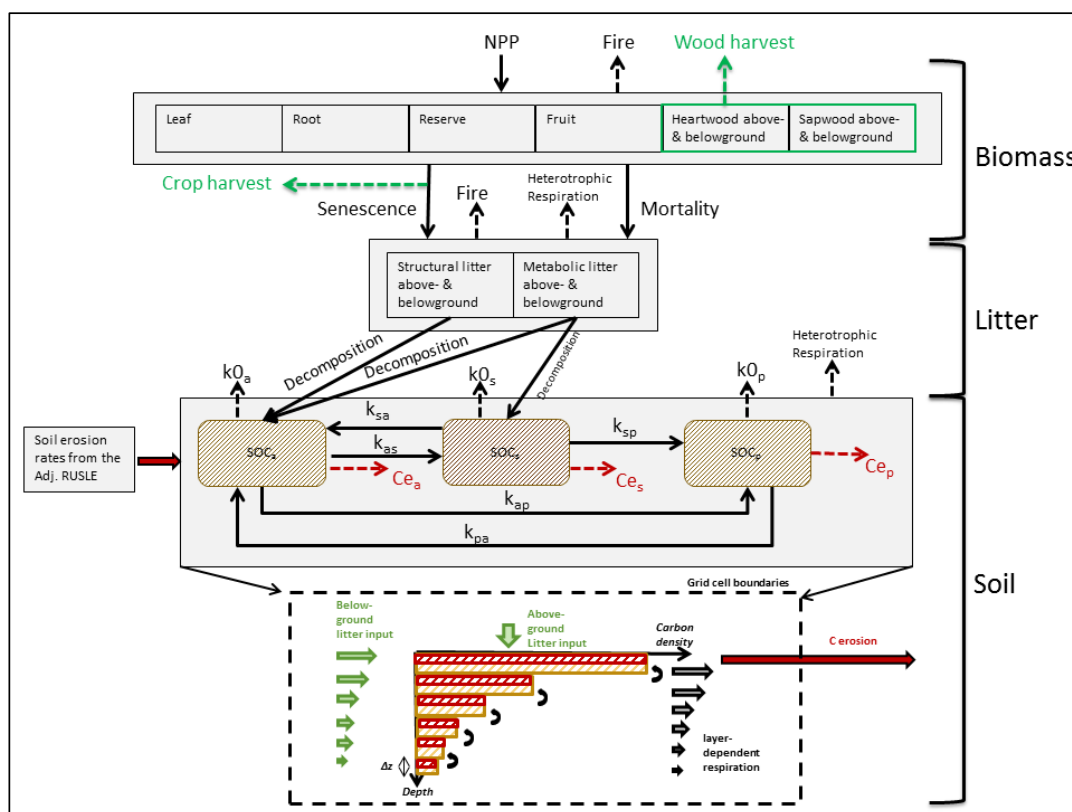
Figure 1(A): The structure of the C emulator (see variable names in the text, paragraph 2.3). The C erosion fluxes are represented by the red arrows and calculated using the soil erosion rates from the Adj.RUSLE model

net land use change

1. Read PFT fractions

2. Identify expanding & shrinking PFT's

3. Collect wood products (wood harvest)

4. Sum the biomass of the area lost of all shrinking PFT's

5. Allocate this to the metabolic/structural litter of expanding PFT's

6. Sum the litter of the area lost of all shrinking PFT's

7. Allocate this to the expanding PFT's

8. Distribute biomass and litter over new PFT area

9. Sum the SOC per soil layer of the area lost of all shrinking PFT's

10. Allocate this to the respective soil layer of the expanding PFT's; In
    this way the SOC soil profile of the expanding and shrinking PFTs
    gets mixed

11. Distribute SOC over new PFT area

Figure 1(B): The land use change module of the emulator
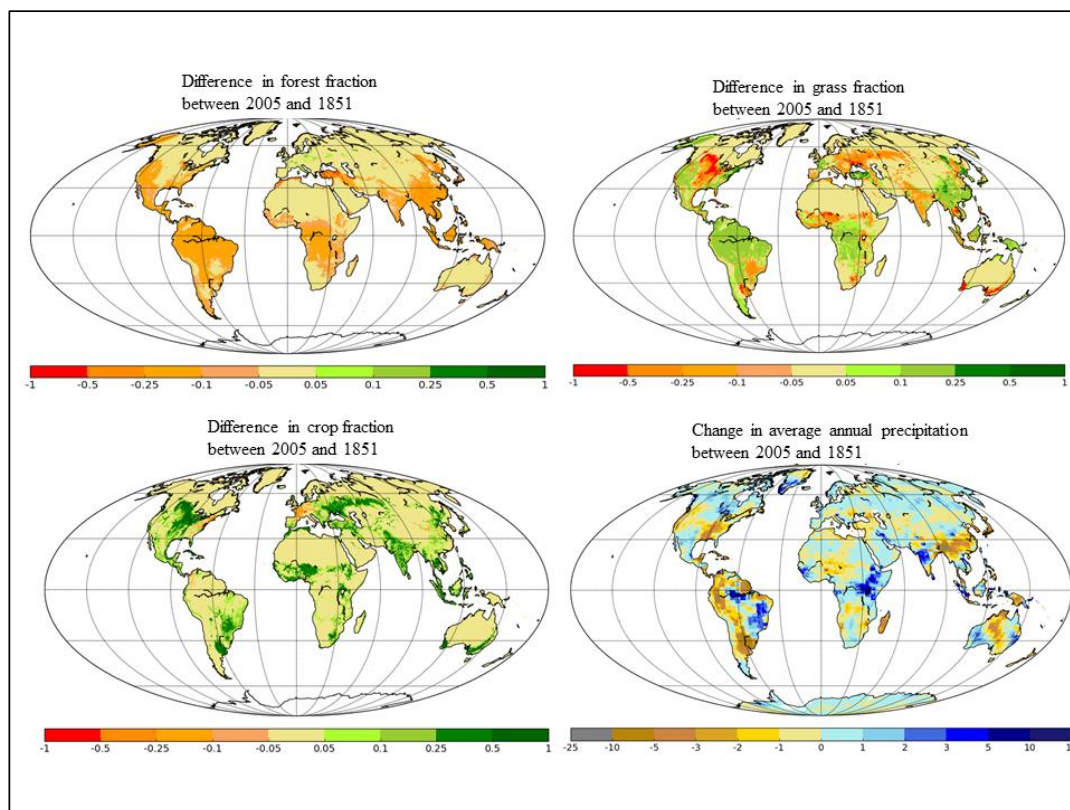
775   Figure 2: Spatial patterns of the difference in forest, crop and grassland area between 1851 and 2005 represented as
a fraction of a grid cell. And spatial patterns of the change in average annual precipitation between 1851 and 2005 in
mm y^{-1}, calculated as the total change in precipitation over the period 1851 – 2005 and divided by the number of
years in this period.
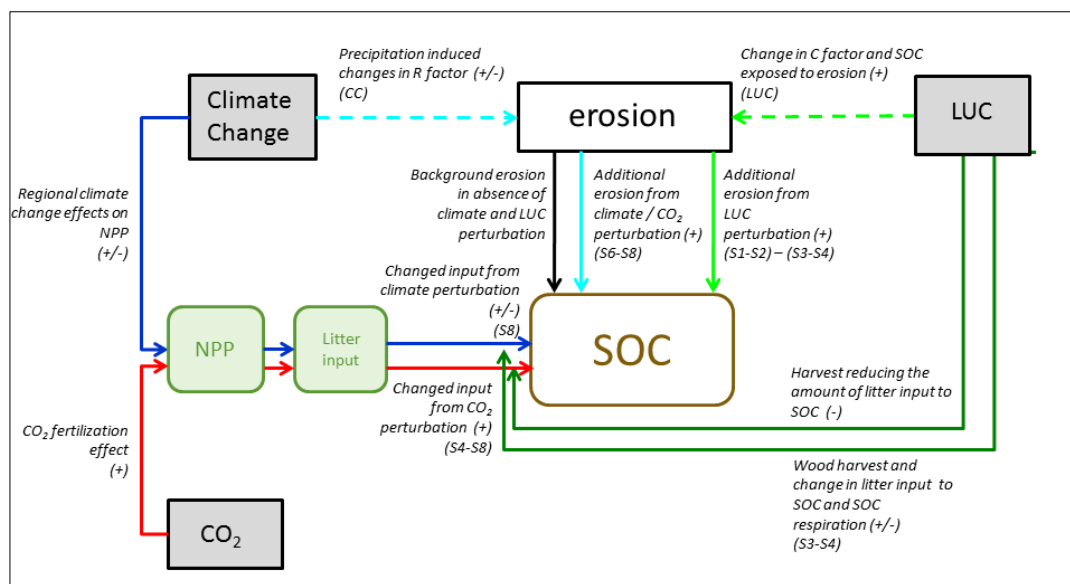
Figure 3: Conceptual diagram of SOC affected by erosion in presence of other perturbations of the carbon cycle,

780   namely climate variability, increasing atmospheric CO_2 concentrations and land use change. A separation of these

components and of the role of erosion is obtained with the factorial simulations (S1-S8), presented in Table 1
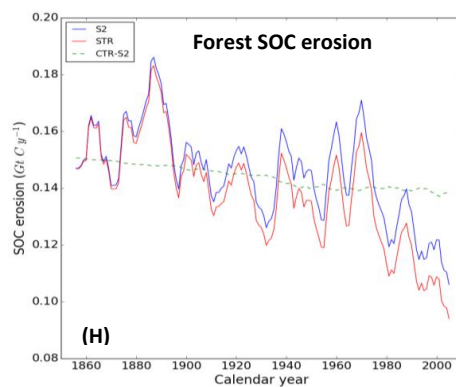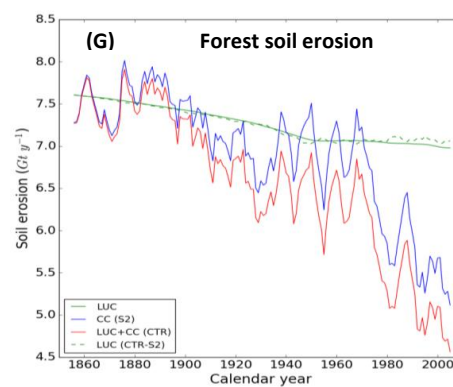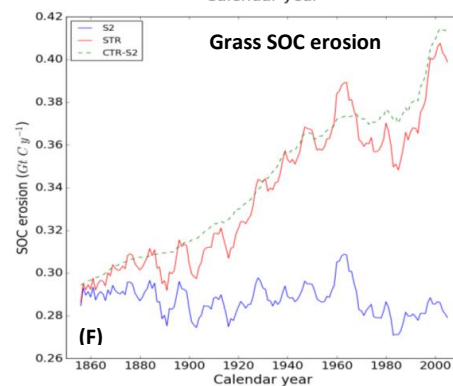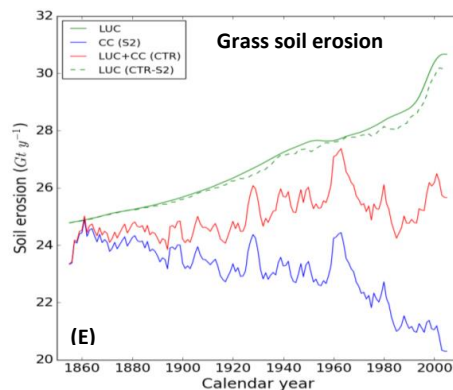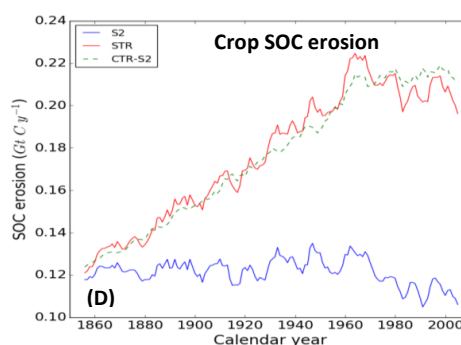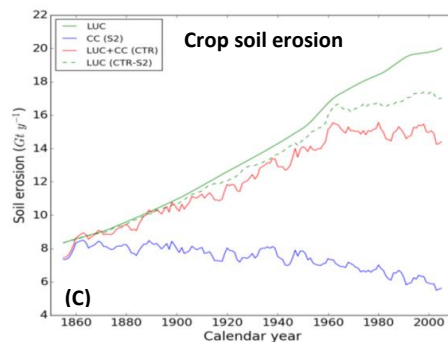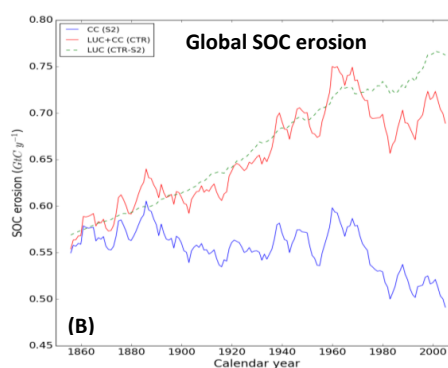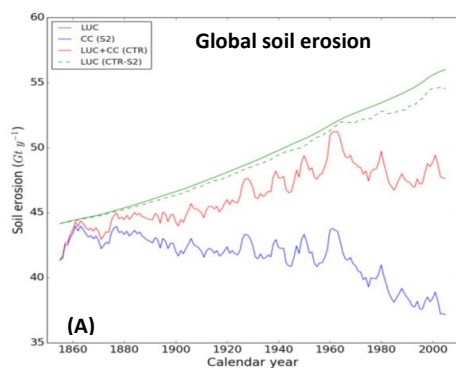
Figure 4: (A) Global annual soil erosion rates, (B) global annual SOC erosion rates, (C) agricultural annual soil erosion rates, (D) agricultural annual SOC erosion rates, (E) grassland annual soil erosion rates, (F) grassland annual SOC erosion rates, (G) forest annual soil erosion rates and (H) forest annual SOC erosion rates over the period 1850-2005 for scenario's with only LUC (green lines), scenario with only climate and CO_2 change (blue line) and scenario with LUC, climate and CO_2 change (red line). In figures A, C, E, and G the dashed green line is the difference between the CTR and S2 simulations, while the straight green line is the LUC-only simulation with the Adj.RUSLE model.
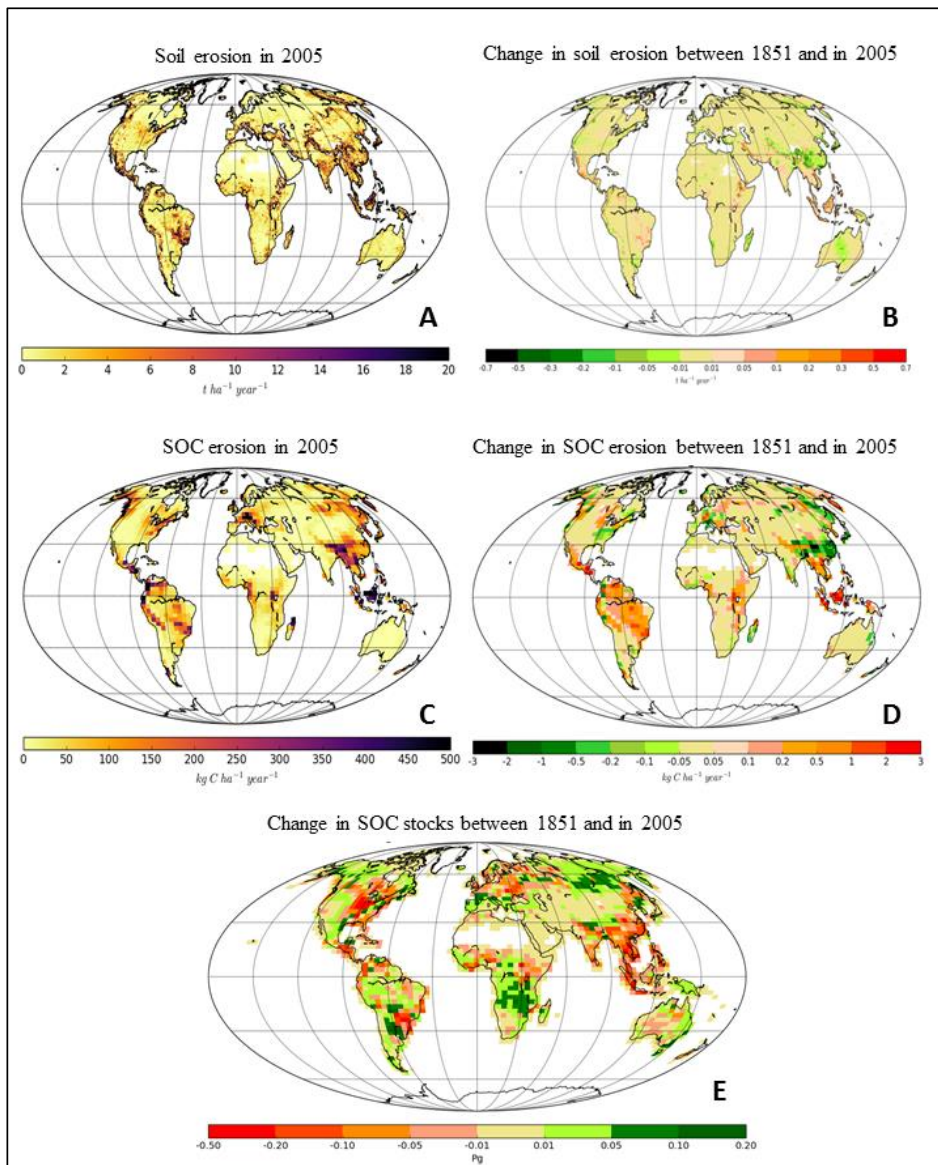
Fig 5: (A) Average annual soil erosion rates at a 5 arcmin resolution in the year 2005, (B) change in average annual soil erosion rates over the period 2005-1850, (C) average annual SOC erosion rates at a resolution of 2.5x3.75 degrees in 2005, (D) change in average annual SOC erosion rates over the period 2005-1850, and (E) difference in
795   SOC stocks at a resolution of 2.5x3.75 degrees between the year 2005 and 1850 (CTR simulation). For the SOC stocks positive values (green color) indicate a gain, while negative values (red color) indicating a loss. For the erosion rates positive values (red color) indicate an increase over 1850 - 2005, while negative values (green color) indicate a decrease over 1850 - 2005
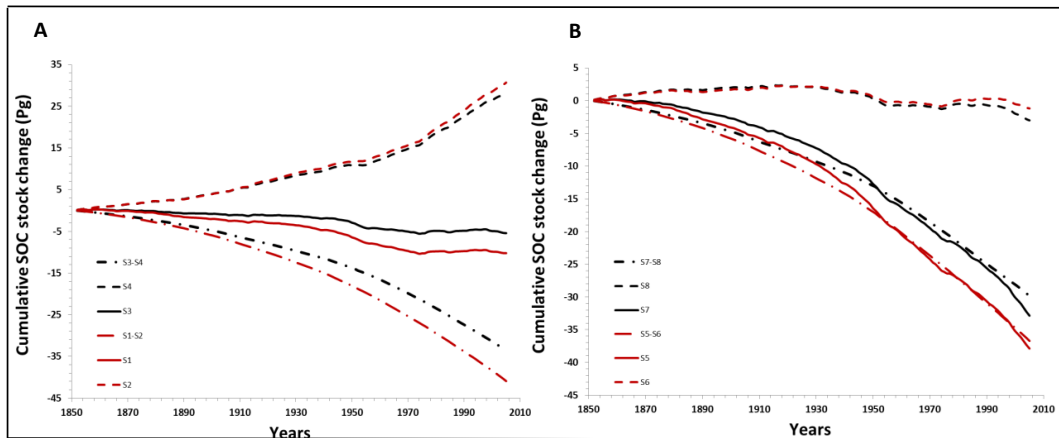
Figure 6: Cumulative SOC stock changes during 1850 – 2005 for (A) simulations with variable atmospheric CO_2
800   concentration, and (B) for simulations with a constant CO_2 concentration, implied by variable land cover alone (dash-dotted lines), by variable climate (dashed lines), and variable land cover and climate (straight lines), without erosion (black lines) and with erosion (red lines).
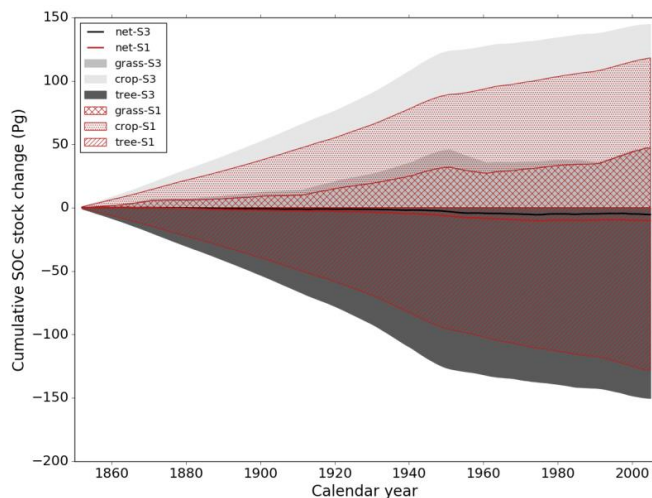
Figure 7: Cumulative SOC stock changes per PFT during 1850 – 2005 implied by variable land cover, climate and CO$_2$, without erosion (grey colors) and with erosion (red colors).

805
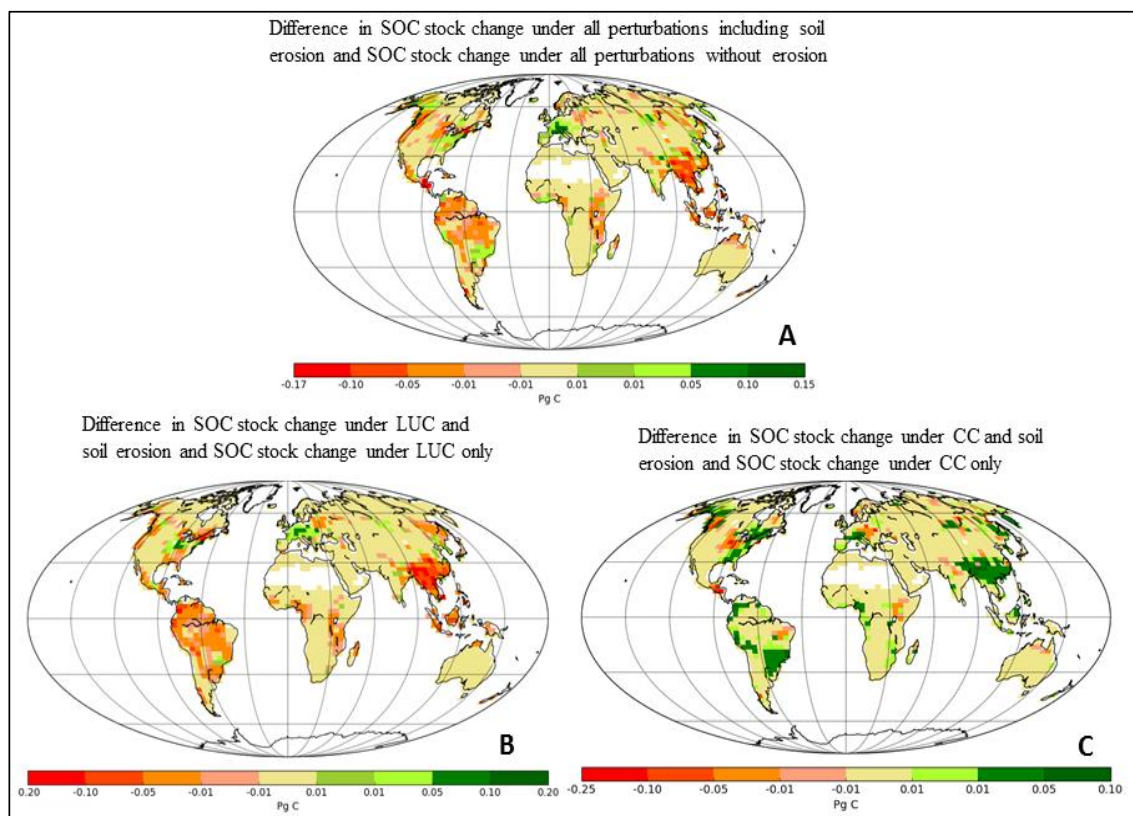
Figure 8: A) Difference between the changes of SOC stocks over the period 1850-2005 under all perturbations including soil erosion and the changes in SOC stocks excluding soil erosion, S1-S3, B) Difference between the changes of SOC stocks under LUC including soil erosion and the changes in SOC stocks excluding soil erosion (S1-S2)-(S3-S4), C) Difference between the changes of SOC stocks under a variable climate and CO$_2$ increase including
810   soil erosion and the changes in SOC stocks excluding soil erosion, S2-S4.
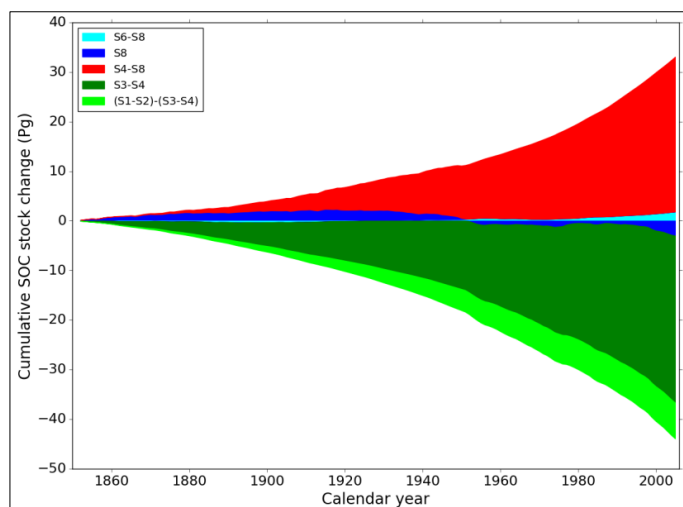
Figure 9: Contribution to the cumulative global SOC stock change over 1850-2005 by CO_2 fertilization (red), effect of precipitation and temperature change on the carbon cycle (dark blue), effect of precipitation change on soil erosion (aqua), LUC effect on the carbon cycle (dark green), and LUC effect on soil erosion (light green)